Energy supply per neuron is constrained by capillary density in the mouse brain

Authors: Lissa Ventura-Antunes[1,2] and Suzana Herculano-Houzel[2,3,4*]

Affiliations:

[1]Instituto de Ciências Biomédicas, Federal University of Rio de Janeiro, RJ, Brazil.

[2]Department of Psychology, Vanderbilt University, Nashville, TN, USA.

[3]Department of Biological Sciences, Vanderbilt University, Nashville, TN, USA.

[4]Vanderbilt Brain Institute, Vanderbilt University, Nashville, TN, USA.

*Correspondence to: suzana.herculano@vanderbilt.edu.

Abstract:
Neuronal densities vary enormously across sites within a brain. Does the density of the capillary bed accompany the presumably larger energy requirement of sites with more neurons, or with larger neurons, or is energy supply constrained by a mostly homogeneous capillary bed? Here we find evidence for the latter across various sites in the mouse brain, such that the ratio of capillary cells per neuron, and thus presumably blood and energy supply per neuron, decreases uniformly with increasing neuronal density across sites. These findings suggest that it is not that larger neurons *demand* more energy, but simply that larger (and thus fewer) neurons have more energy available per cell than smaller (and thus more numerous) neurons due to competition for limited resources supplied by capillaries.

One Sentence Summary: Limited blood supply gives larger neurons a competitive edge for more energy over smaller neurons, with implications for brain evolution and healthy aging

INTRODUCTION

Of the organs of the human body, the brain is second in absolute energy cost only to the liver (*1,2*). Such high cost is commonly attributed to synaptic-mediated neuronal activity (*3-5*) and is entirely dependent on molecules supplied from the blood and provided to neurons through glial cells whose metabolism is coupled to neuronal activity (*6,7*). The dependency of local brain metabolism on the capillary blood supply is evidenced by the finding that at rest, both local glucose use and blood flow depend linearly on local capillary density in rat (*8*) and monkey (*9*). Moreover, the high energy cost of organs such as the brain, liver and heart puts them at high risk of damage by diseases, insults, and other conditions, such as aging, that compromise metabolism

and/or energy and oxygen supply (*10*). Elucidating what determines the high energetic cost of the brain is thus central to understanding healthy and abnormal brain function.

Brain bioenergetics researchers typically consider that the high energetic cost of the brain is driven by the steep energetic requirement of neurons, due to costs, directly and indirectly, related to synaptic activity and membrane repolarization (*3-7,11,12*). It is also expected that larger neurons have more synapses and, thus, a higher energetic cost than smaller neurons (*3*). However, *a priori*, energetic cost can be determined either by energetic *demand* that is matched dynamically by a non-limiting supply (as in the electricity that supplies homes in modern cities) or by a limited energetic *supply* that constrains work (as in rural homes that cannot sustain both an electric shower and air conditioning running simultaneously, or in hummingbirds that enter torpor when food is insufficient) (*13,14*). In the case of the brain, the task-dependent variation in local perfusion rate (measured as cerebral blood flow, CBF) is consistent with alterations in energy demand related to neuronal activity, even if these local changes in CBF are not necessarily accompanied by increased rates of oxygen use (reviewed in [*15*]). Additionally, task-related variation in CBF is very small, in the order of 2%, and of at most 8% in primary sensory areas (*16,17*).

Most importantly, variation in blood perfusion rates across sites happens in a context of constant blood volume in the brain as a whole, that is, without capillary recruitment (*18*). Small task-dependent local variations in blood flow rate are therefore more consistent with brain metabolism being constrained mostly by a limited supply of energy depending on capillary density (*14*) than met with variable supply according to energetic demands. Thus, while neuroscientists often frame the energy *cost* of the brain in terms of high neuronal *demand* for energy, it is helpful to reframe energy "cost" as simply energy *use*, a term that implies nothing about what defines it, whether supply or demand and instead leaves these open to investigation. The issue of energetic *use* by neurons can then be separated into the more tractable questions of (a) whether there is evidence that larger neurons *demand* more energy, depending on their intrinsic biophysical properties, as proposed in (*3*), and (b) whether there is evidence that larger neurons are *supplied* with more energy than smaller neurons, regardless of (a).

A necessary first step to establishing whether larger neurons *use* more energy, be it due to increased demand, supply, or both, is comparing average energy use per neuron where neurons have different sizes, both within and across species. The practical impediment here is that

measuring energy use requires bringing live animals to the lab. There are presently no direct data available on rates of energy use per neuron, whether in different structures or species, to test the hypothesis that larger neurons use more energy (whether due to supply or demand); all measurements so far have been of energy use per gram of tissue (*19,20*), not per neuron.

The limitations to studying energy use per neuron in living animals could be overcome if there was a viable alternative to estimating energy availability in fixed brain tissue. Local capillary density, which correlates very well, and linearly, with blood flow and local rate of glucose use at rest in both rat (*8*) and macaque brains (*9*), can be measured in fixed brains. While the dynamic variation of blood flow rates does occur at the level of arterioles and capillaries (*15*), the lack of a consistent correlation of this dynamic variation with rates of oxygen use reviewed above begs the question of how the capillary blood supply alone relates to neuron distribution and thus might be limiting to neuronal activity.

To that end, here we estimate energy availability per neuron as gauged through the local endothelial-to-neuronal-cell (E/N) ratio and how it varies locally in the mouse brain by measuring local densities of capillary cells and neurons across multiple sites and structures with different neuronal densities. To examine whether variations in energy availability per neuron might also be related to local variations in numbers of synapses per neuron, as expected in the demand-based framework of brain metabolism, we also combine our data with direct counts of synapse densities in identified locations in the mouse brain published recently (*21*) to perform a similar analysis of endothelial-cell-to-synapse ratios (E/S) and synapse-per-neuron ratios (S/N) in relation to E/N and thus establish whether local variations in the distribution of capillaries accompany local variations in neuronal density, in synaptic density, or neither. Fig. 1 portrays two examples of how our findings would correspond to different scenarios (more possible scenarios in Fig. S1). If individual neurons demand a constant amount of energy that is similar across sites regardless of neuronal cell size, then local densities of capillary cells should vary accompanying local neuronal densities, and E/N should be constant across the brain sites (Fig. 1, row 1). On the other hand, if larger neurons use more energy, then sites with larger neurons and thus lower neuronal densities should have higher E/N (Fig. 1, row 2); however, more energy per neuron due to neuronal *demand* would also require variable capillary densities depending on local neuronal size, and thus density (Fig. S1, rows 3 and 4). In contrast, if larger neurons are supplied more energy simply by virtue of there being fewer neurons competing for local blood

supply, then sites with larger neurons and thus lower neuronal densities should have higher E/N, but in the absence of significant, systematic variations in capillary density (Fig.1, row 2).

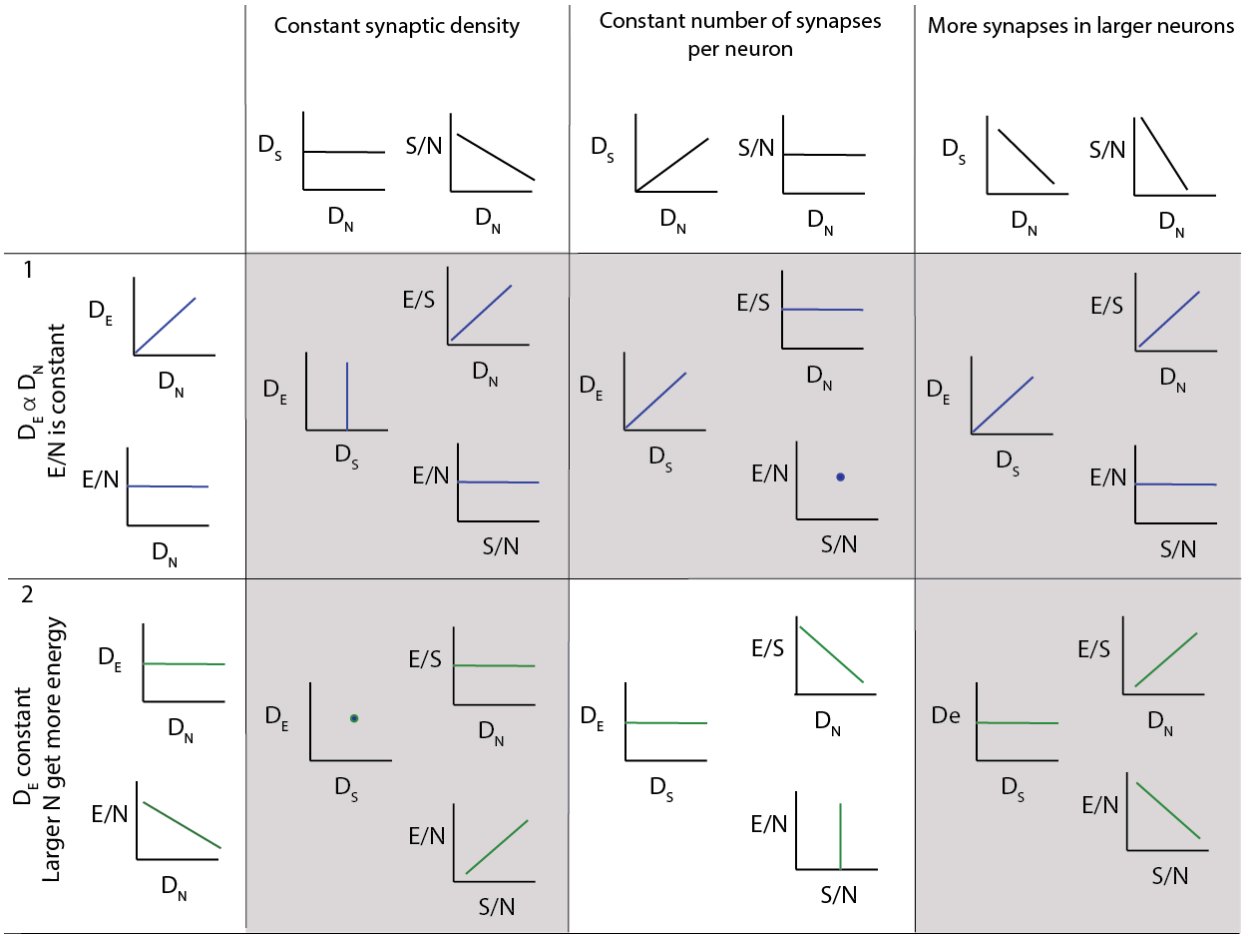

Fig 1. Two of several possible scenarios of relationships among local density of capillary cells (D_E), local density of neurons (D_N), energy available per neuron (E/N, estimated as D_E/D_N), local density of synapses (D_S), average number of synapses per neuron (S/N) and average energy supply per synapse (E/S). Scenario 1 (top row): neurons demand a certain fixed supply of energy, and the capillary bed adjusts to supply it at a steady-state, such that energy supply per neuron is constant across sites. In this scenario, D_E is expected to be proportional to D_N, and energy available per neuron (E/N) is constant. **Scenario 2 (second row)**: capillary supply to brain tissue is constant across sites, and neurons compete for whatever energy is available. In this case, D_E is expected to be relatively constant regardless of local D_N; as a result, E/N is larger in sites of lower neuronal densities (indicative of larger neurons), where fewer neurons compete for a limited supply of energy. This is the scenario supported by our findings, but incompatible with current models. **Columns** indicate, for each scenario of capillary and neuronal distribution, the expected findings regarding variations across the variables measurable in this study depending on whether **(left column)** local synaptic densities are mostly constant across sites, such that there are more synapses per neuron where neurons are larger (and D_N lower); **(center column)** the number of synapses per neuron is mostly constant, such that there are more synapses where there also are more neurons; and **(right column)** larger neurons have many more synapses than smaller neurons, such that local synaptic densities are larger where neurons are larger (and D_N lower). Our findings support a constant density of capillaries with fairly constant densities of synapses per neuron, such that energy supply both per neuron and per synapse, and thus energy availability per

neuron and per synapse, decreases the higher the local neuronal density, that is, the smaller the average local volume of individual neuronal cells. This is the scenario highlighted.

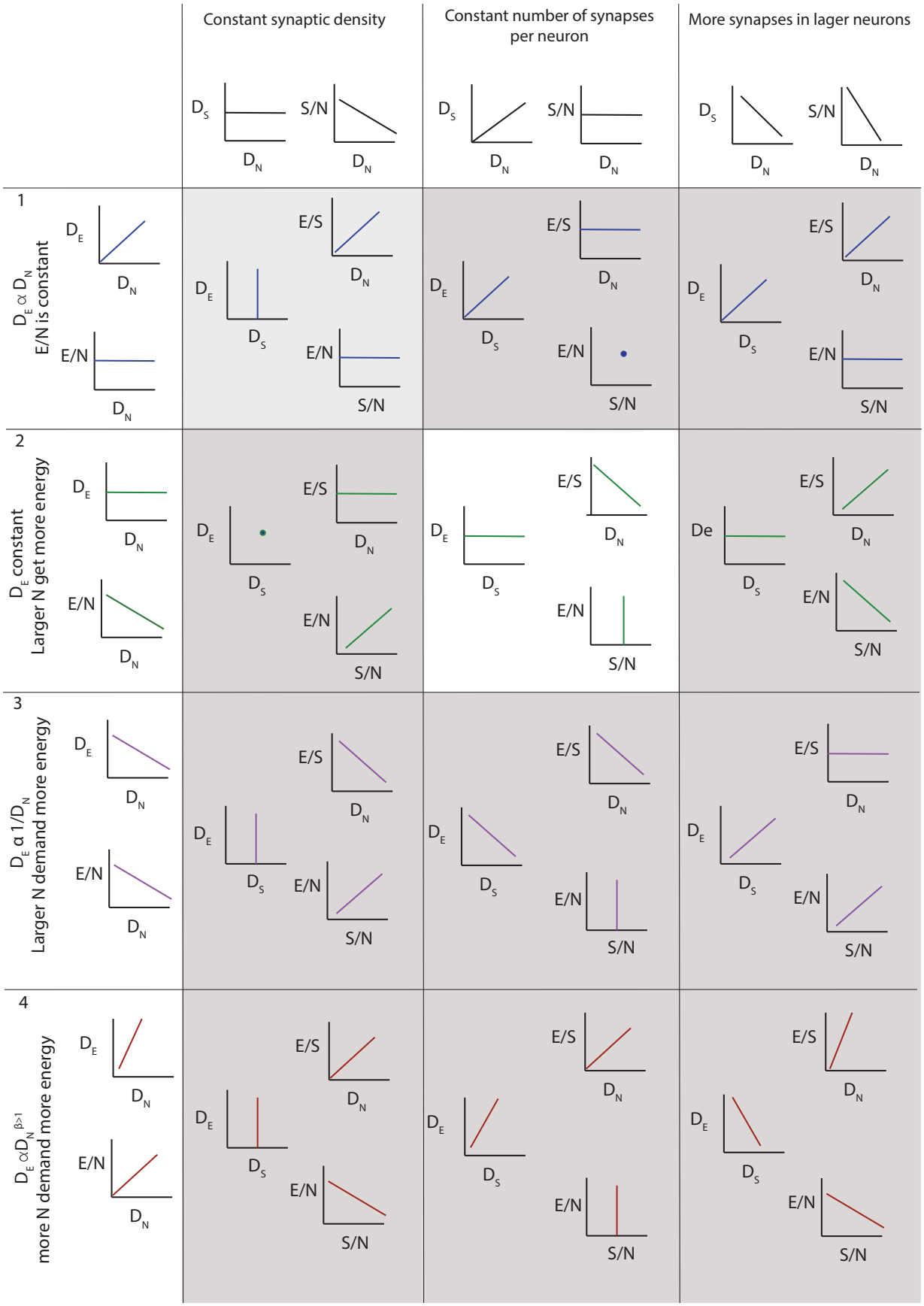

Fig S1. Possible scenarios of relationships among local density of capillary cells (D_E), local density of neurons (D_N), energy available per neuron (E/N, estimated as D_E/D_N), local density of synapses (D_S), average number of synapses per neuron (S/N) and average energy supply per synapse (E/S). Scenario 1 (top row): neurons demand a certain fixed supply of energy, and the capillary bed adjusts to supply it at a steady-state, such that energy supply per neuron is constant across sites. In this scenario, D_E is expected to be proportional to D_N, and energy available per neuron (E/N) is constant. **Scenario 2 (second row)**: capillary supply to brain tissue is constant across sites, and neurons compete for whatever energy is available. In this case, D_E is expected to be relatively constant regardless of local D_N; as a result, E/N is larger in sites of lower neuronal densities (indicative of larger neurons), where fewer neurons compete for a limited supply of energy. This is the scenario supported by our findings, but incompatible with current models. **Scenario 3 (third row)**: larger neurons demand more energy, and the capillary bed adjusts to supply it, such that energy supply per neuron is larger where neurons are also larger, and thus occur at lower D_N. This scenario is compatible with current models (*3-5*), but is not supported by our present findings. **Scenario 4 (bottom row)**: energy supply per neuron increases more rapidly than whatever energy is demanded per neuron, such that energy availability (E/N) is higher the more neurons are present locally. This is the only scenario in which energy supply is not limiting, neither in practice nor in theory. **Columns** indicate, for each scenario of capillary and neuronal distribution, the expected findings regarding variations across the variables measurable in this study depending on whether **(left column)** local synaptic densities are mostly constant across sites, such that there are more synapses per neuron where neurons are larger (and D_N lower); **(center column)** the number of synapses per neuron is mostly constant, such that there are more synapses where there also are more neurons; and **(right column)** larger neurons have many more synapses than smaller neurons, such that local synaptic densities are larger where neurons are larger (and D_N lower). Our findings support a constant density of capillaries with fairly constant densities of synapses per neuron, such that energy supply both per neuron and per synapse, and thus energy availability per neuron and per synapse, decreases the higher the local neuronal density, that is, the smaller the average local volume of individual neuronal cells. This is the scenario highlighted.

RESULTS

We quantified capillary area fraction (which is identical to capillary volume fraction), and cell densities in ten easily definable brain structures (cerebral cortical gray and white matter, cerebellar gray and white matter, thalamus, hypothalamus, striatum, hippocampal and cerebellar granular and molecular layers) imaged with structured confocal illumination in a total of 5 mice, comprising 867 stacks analyzed in 3D (two mice, total of 32,270 cells) and 750 ROI acquired and analyzed in 2D (three mice, total of 196,206 cells; Tables S1, S2; see Methods). While image stacks allow detailed visualization of microvasculature in 3D, two-dimensional analysis of image montages allows for larger sites with larger cell populations to be sampled in less time (Fig. S2). We thus compared the two approaches in this study to determine whether 2D analysis of the distribution of capillaries and neurons are a viable and more efficient alternative to 3D quantification. From all DAPI-labeled cell nuclei in each stack or 2D ROI, we identified all NeuN-positive cell nuclei as neurons; all nuclei directly associated with collagen IV-labeled or FITC-dextran filled capillaries as endothelial and associated cells (which includes eventual pericytes; heretofore, "endothelial cells"), and by elimination, all remaining nuclei were deemed glial cells (Fig. S3). Cell densities were calculated as cell nuclei per mm^3 or mm^2, depending on

the stack volume or ROI area analyzed to include capillaries only. All results are shown side by side in 2D and 3D analyses.

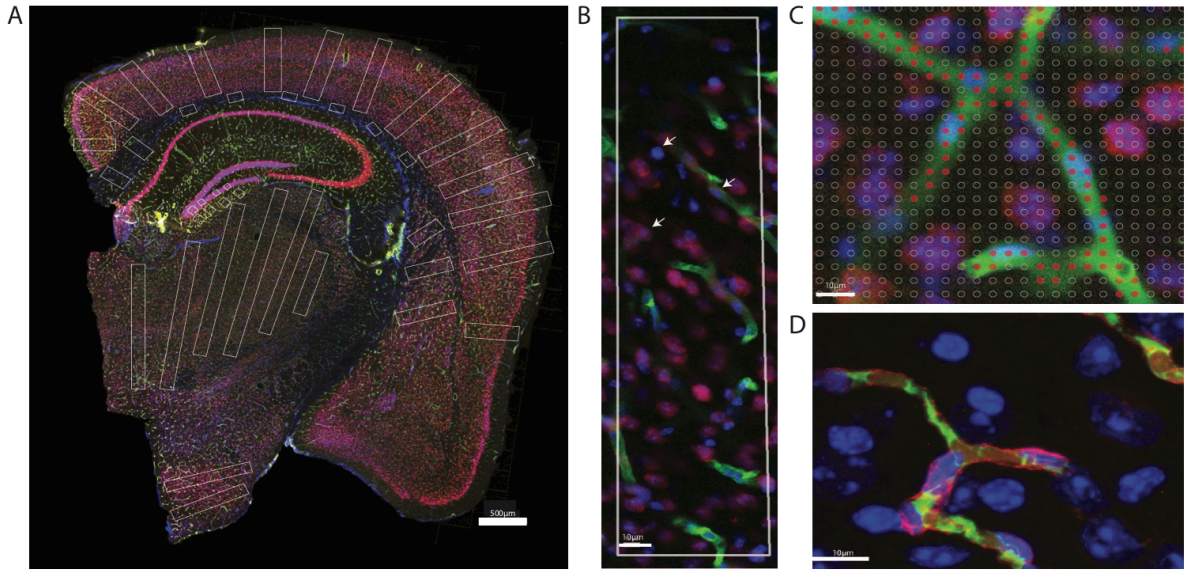

Fig. S2. Two-dimensional image analysis. A. Areas sampled for 2D quantification are shown in white across structures in a coronal section of the mouse brain. Scale bar, 500 µm. **B.** ROI in the cortical gray matter showing microvasculature labeled with anti-collagen IV (green), neurons labeled with anti-NeuN (red) and Dapi to reveal all cell nuclei (blue). Cell nuclei appearing inside green-labeled blood vessels are considered capillary-associated nuclei; cell nuclei double-labeled in red are considered neuronal cell nuclei; all remaining nuclei are identified by exclusion as glial cell nuclei. **C.** A Cavalieri estimator grid of 4 µm spacing (shown) was applied to images acquired under 20x magnification, and a 2µm grid was applied to images acquired under 63x magnification. The points marked in red correspond to the area of the image occupied by capillaries. Scale bar, 10µm **D**. Superposition of FITC-dextran (green, lumen) and collagen IV (red, basal lamina) labeling of capillaries. Single image acquired under 63x magnification. Scale bar, 10µm.

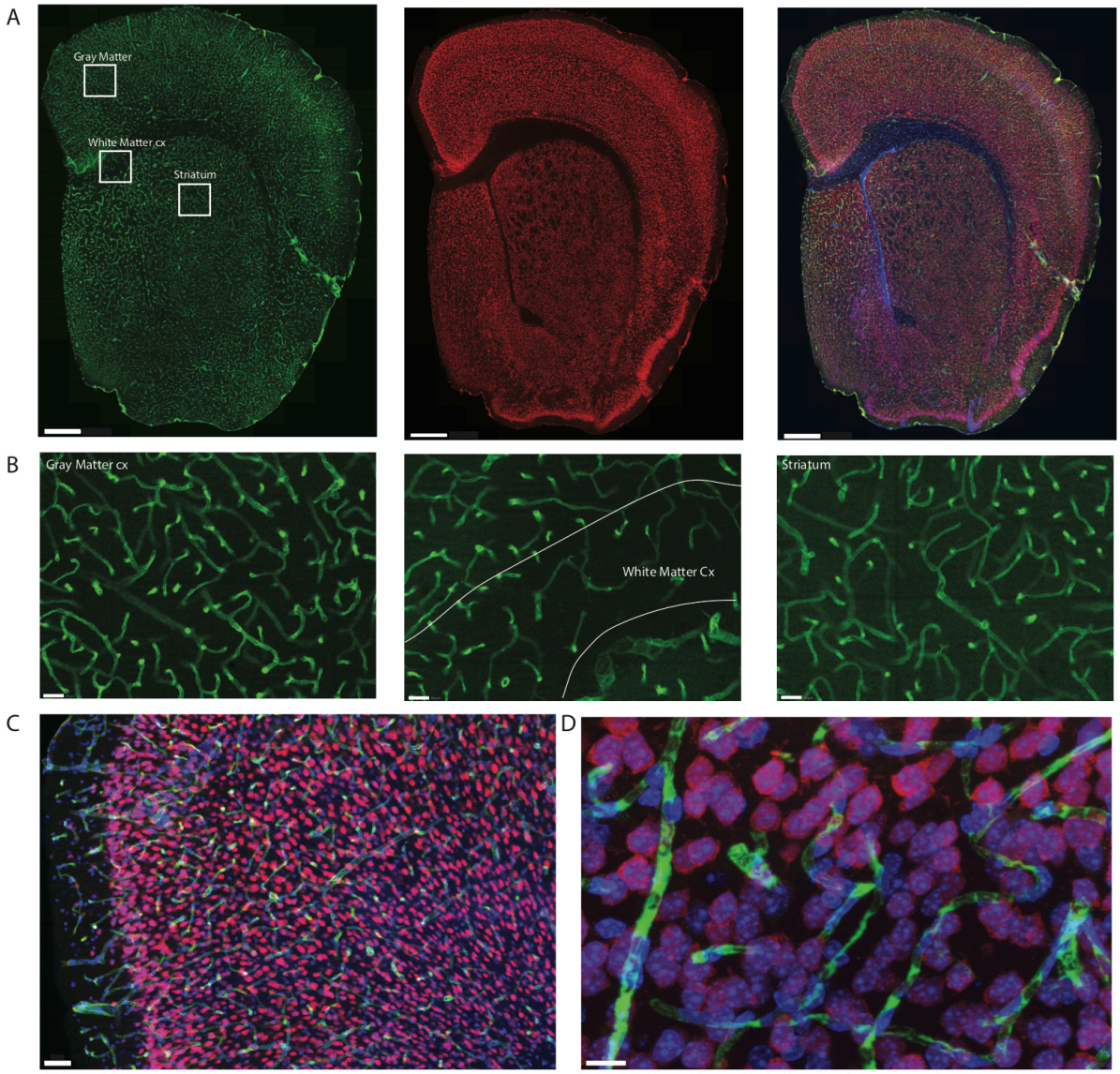

Fig. S3. Example of triple labeling for vasculature, neurons, and all cell nuclei. Shown is a coronal section of a mouse brain label by systemic injection of FITC-Dextran. A. Coronal section of mouse brain showing microvasculature labeled with injection of FITC-dextran (left, green), neuronal nuclei labeled with NeuN-Cy3 (center, red), and all nuclei labeled with DAPI (right, blue in merged images). Scale bar, 400µm. **B.** Zoom of insets in A using the 63x objective with the thinner depth of field illustrating the extent of differences in capillary densities across brain sites. Scale bar, 50 µm. **C.** Section through cortical gray matter under 20x magnification stained to reveal Collagen IV (green), NeuN (red) and cell nuclei (blue). Scale bar, 50 µm. **D.** Maximal projection image of 3D stack through cortical gray matter imaged under 63x magnification. Scale bar, 10µm.

Across the ten brain structures examined, we find that the capillary area fraction is very small, amounting to no more than 3% of the tissue in any structure in 3D image stacks. While individual measurements of local capillary fraction vary 10x-fold across all brain sites, the average capillary fraction per structure varies only about 2-fold across structures, with 95% of measurements ranging around 1.29 ± 1.39% (Table S3). The average capillary fraction is highest in the gray matter of the cerebral cortex (2.22±0.11%), and lowest in the granular layer of the dentate gyrus and subcortical white matter (0.70±0.07%; Table S3). In 2D images, we found similarly small variation in capillary fraction, as well as lower capillary fractions in white matter than in gray matter, despite the artificially higher nominal capillary fractions measured with this method due to the larger optical thickness of the images (Table S4). The capillary fractions we report in 3D analyses are similar to vascular fractions between 2% and 6% reported in the mouse cerebral cortical grey matter (*22*) and between 2.1% and 3.1% in the cat, macaque and human gray matter cortex (*23-25*).

Interestingly, capillary-associated ("endothelial") cells typically constitute between 7 and 14% of all cells forming the brain structures examined (Tables S3, S4), a much larger percentage than could be expected from the average vascular fraction of 0.7-2.2% of the 3D volume that they occupy. This discrepancy indicates that endothelial cells are, on average, much smaller than neurons and glial cells in the tissue. Still, glial cells are consistently the majority (at least 60-70%) of non-neuronal cells in all structures (Tables S3, S4). As expected from our previous studies (*26*), the percentage of cells that are neurons is highly variable across structures and sites within a structure; neurons are the vast majority of all cells in the granular layers of the dentate gyrus and cerebellum, a smaller percentage of all cells in other gray matter structures, and rare (but present) within the subcortical white matter of both cerebral and cerebellar cortices (Tables S3, S4).

As expected for two different measurements of the same feature (capillary density), local endothelial cell density correlates well with local capillary area or volume fraction within and across the different brain structures, as well as across animals, especially in the 2D sample, which included a much larger number of sites and cells (Fig. 2A; Table S1). Both capillary fraction and local endothelial cell density vary by a single order of magnitude across sites in the mouse brain, whether measured in 2D or 3D (Fig. 2A). The two capillary density-related variables are correlated within each structure individually (Table S5), and there is good overlap

in data points across structures and animals, especially in the larger 2D dataset (Fig. 2A, right), where the overlapping power relationships (Table S5) indicate that the relationship between capillary fraction and cellular composition of capillaries is shared throughout the brain. This agreement suggests that endothelial cell density is a good proxy for the resting rates of blood flow and glucose use (*8,9*).

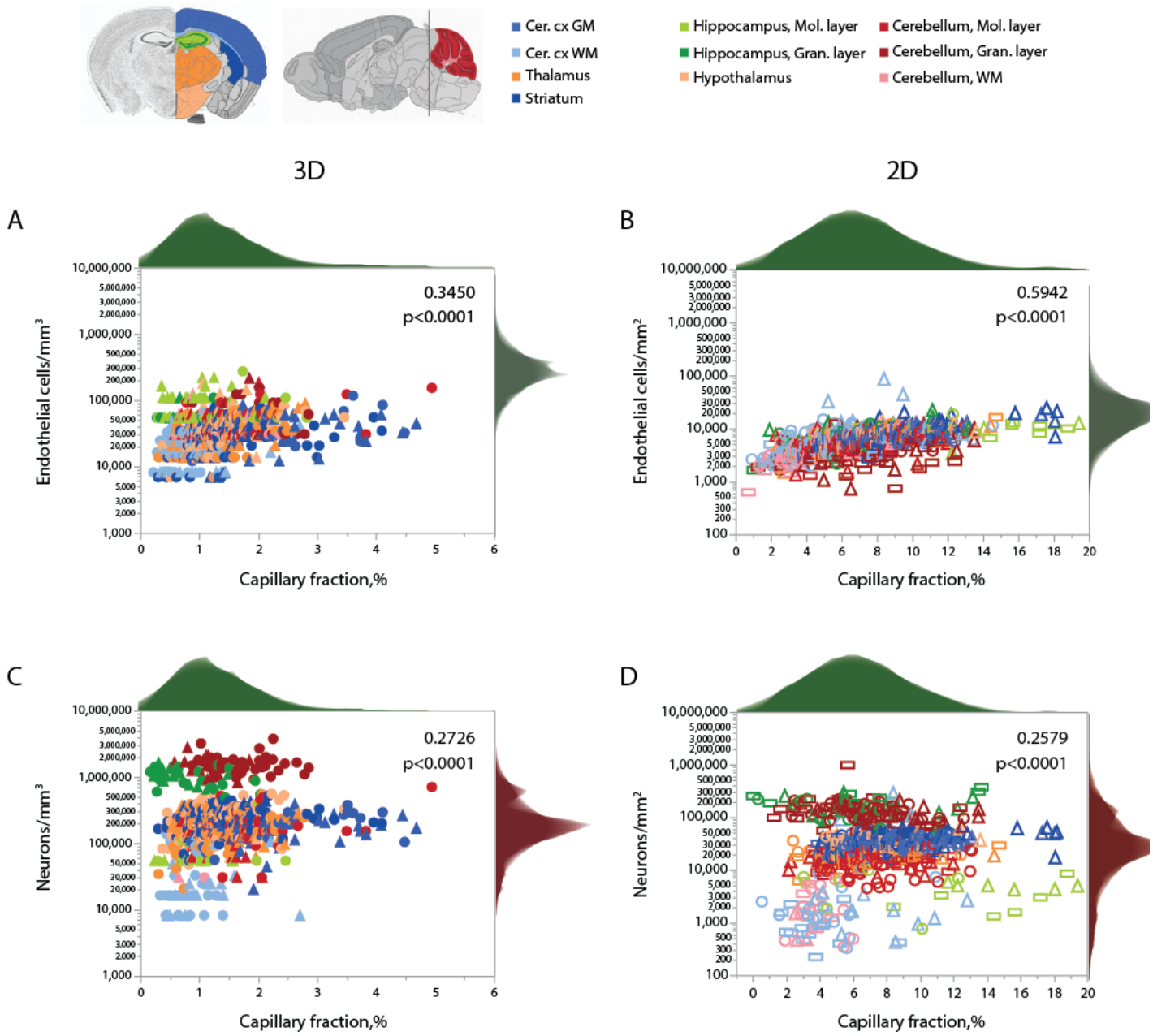

Fig. 2: Local capillary fraction correlates with local endothelial cell density, but not with neuronal cell density. A, B: Local density of endothelial cells correlates with local vascular fraction across all sites and structures

analyzed in 3D (**A**; two animals, shown in circles or triangles, left) and in 2D (**B**; three animals, shown in circles, triangles, or rectangles, right) with the Spearman correlation coefficients and p-values across all animals and sites indicated in each graph. **C, D:** In contrast, local neuronal density does not correlate significantly with local vascular fraction across brain sites and structures in 3D (**C**) or in 2D (**D**). Histograms above and to the right reflect the distribution of all data points in each axis. Graphs in **A/C** and **B/D** are shown with similar X and Y scales for comparison. Correlation coefficients and power exponents for each structure are given in Table S5.

Neuronal densities, in contrast, vary over two orders of magnitude across sites in gray matter structures, from 31,250 to 3,843,750/mm^3 (Fig. 2B), and are not significantly correlated with local capillary fraction (Figure 2B) across brain sites and structures. In fact, brain structures with enormously different neuronal densities have capillary fractions in the same restricted range (Fig. 2B), and correlations, where significant, can be positive (cortical GM) or negative (cerebellar granular layer; Table S5).

Like endothelial cell densities, variation in glial cell densities is restricted to within one order of magnitude across sites in the mouse brain (Fig. 3A). Within the cortical gray matter, local glial cell densities vary significantly in positive correlation with local neuronal density, as previously observed across sites within both human (*27*) and mouse (*28*) cortices (Fig. 3A; Table S5). In contrast, there is no universal correlation between local neuronal and glial cell densities across brain structures; if anything, there is a modest negative correlation across all sites (Fig. 3A), which is due to the slightly more elevated glial cell densities in white matter sites.

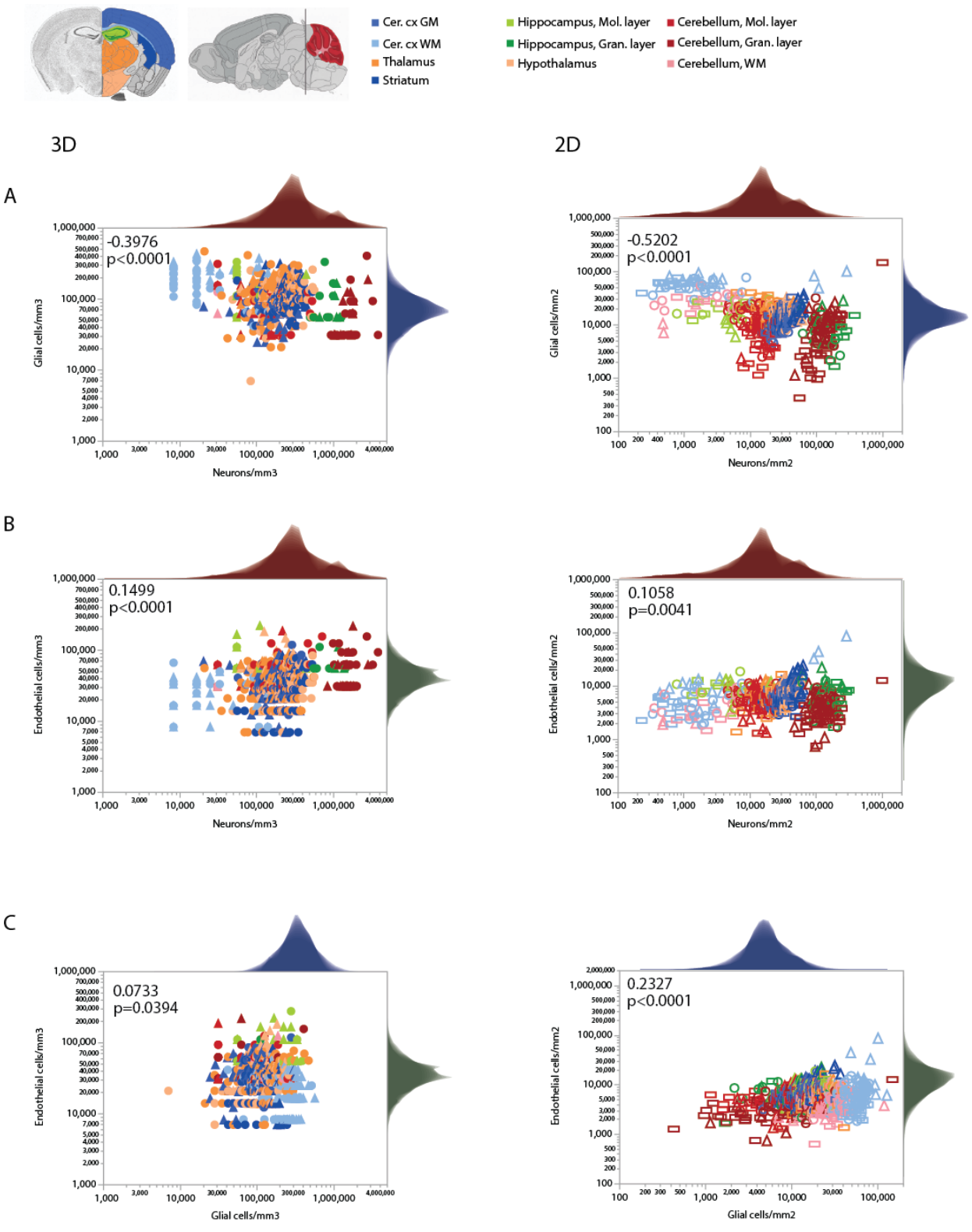

Fig. 3. Local densities of different cell types vary concertedly only within some brain structures. Each plot is accompanied by the respective distribution histograms aligned with the X and Y axes. Spearman correlation coefficients and p-values across all structures and sites are indicated in each graph. **A.** Glial cell densities span just

over one order of magnitude across structures, while neuronal cell densities span two orders of magnitude. While the correlation across all data points is significant and negative in both 3D and 2D datasets, analysis at that level ignores obvious differences across structures (see Table S4). **B.** Similarly, endothelial cell densities are concentrated within one order of magnitude across structures and sites, and are similar across structures with very different neuronal densities. Still, local endothelial and neuronal cell densities are significantly and positively correlated within the cortical gray matter, the thalamus, and the striatum (see Table S4). **C.** Glial and endothelial cell densities, which vary little across sites and structures in comparison to neuronal densities, are not strongly correlated across brain structures, and weakly correlated within some (see Table S5). All graphs are shown with similar X and Y scales for comparison.

Importantly, a large range of neuronal densities occurs with fairly similar endothelial cell densities across structures in the mouse brain, with only a weak overall trend toward higher endothelial cell densities where neuronal densities are higher (Fig. 3B). A significant increase in local endothelial cell density in sites with increasing local neuronal density is found only in the cortical gray matter, thalamus and striatum (Fig. 3B, Table S5). Similarly, we find significant correlations between local densities of endothelial cells and glial cells within some structures, but no strong systematic correlation across locations (Fig. 3C).

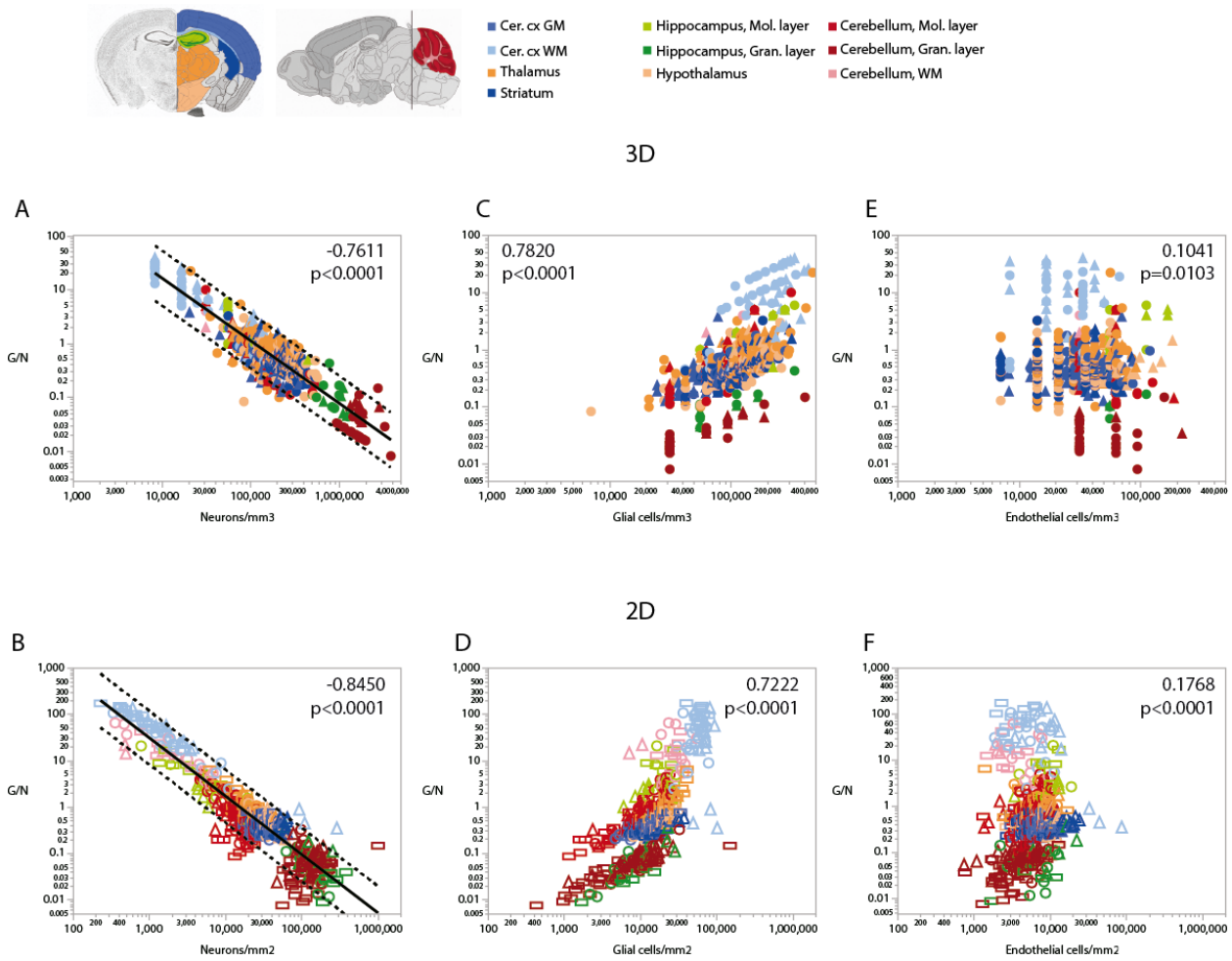

Fig. 4. Ratio of glial cells per neuron (G/N) increases across brain structures and sites with decreasing neuronal densities. Spearman correlation coefficients and p-values across all structures and sites are indicated in each graph; relationships for each structure are given in Table S4. G/N ratios span over three orders of magnitude and vary as a single power function of neuronal density across all brain structures and sites whether measured in 3D stacks (**A**) or in 2D composite images **(B).** Power functions are plotted with 95% confidence interval (dashed lines), and have exponents -1.162±0.024, r^2=0.816, p<0.0001 (**A**, 3D) or -1.257±0.020, r^2=0.865, p<0.0001 (**B**, 2D). Notice that most data points in all structures are contained within the 95% CI of the function that applies across structures, indicating that the relationship is brain-wide. **C, D:** G/N ratio also correlates with glial cell densities across all brain structures and sites, but the relationships are clearly distinct across sites (see exponents in Table S4). **E, F:** Although a weak correlation is detected between G/N ratios and endothelial cell densities across brain structures and sites, most local correlations are non-significant or weak, with a wide range of non-overlapping values of G/N for similar endothelial cell densities across brain structures. All graphs are shown with similar X and Y scales for comparison. Correlation coefficients and power exponents for each structure are given in Table S5.

Consistently with the larger variation of neuronal densities than glial cell densities across locations, the glia/neuron (G/N) ratio is highly variable within the mouse brain, and is universally and inversely related to local neuronal densities across all sites and structures (Fig. 4A, B). That is, there are more glial cells per neuron in those sites with lower neuronal densities, in a relationship that applies both across and within structures, regardless of their identity (Table

S5). In contrast, the relationship between local glia/neuron ratio and glial cell density is specific to each structure, with different ranges of glia/neuron ratios sharing similar glial cell densities across structures (Fig. 4C, D). Importantly, although higher G/N ratios where neuronal densities are smaller (and therefore neurons are larger) have been proposed to accompany the presumably higher energetic demands of larger neurons (*3, 4*), the entire 10,000-fold range of G/N ratios occurs within the same restricted range of endothelial cell densities, with no consistent correlation across brain structures and sites (Figure 4E, F). That is, endothelial cell densities are not significantly higher in those locations where each neuron is accompanied by a larger number of glial cells.

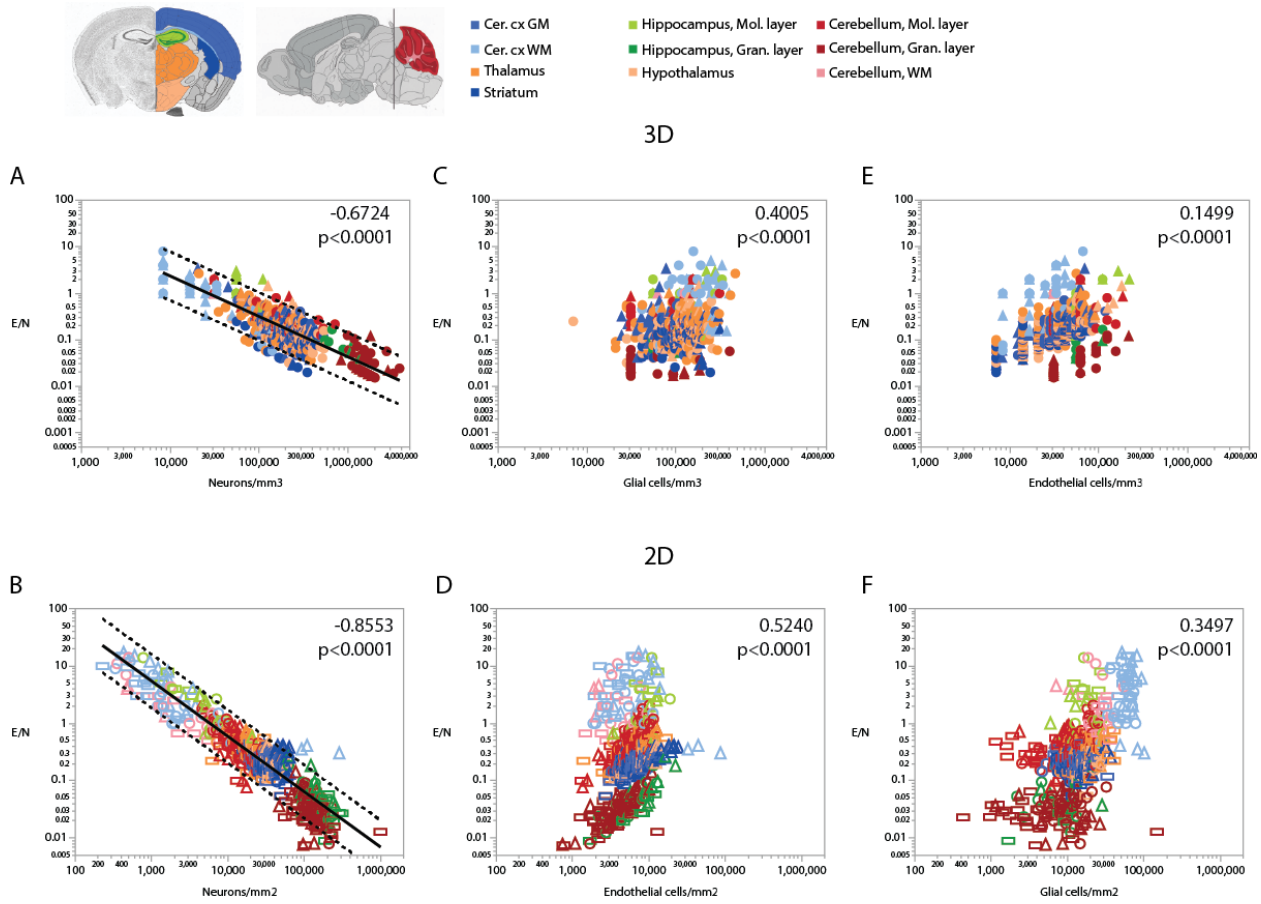

Fig. 5. Ratio of endothelial cells per neuron (E/N) varies widely and uniformly across brain structures and sites depending on local neuronal density, but correlations with glial and endothelial cell densities only apply locally. Spearman correlation coefficients and p-values across all structures and sites are indicated in each graph; correlations and power function exponents for each structure are listed in Table S4. **A, B:** E/N ratios span three orders of magnitude across brain sites and structures and vary as a single power function of local neuronal density whether measured in 3D stacks (**A**) or in 2D composite images (**B**). **C, D:** E/N ratio appears to correlate with local glial cell density across brain structures in both datasets, but closer inspection reveals that the overall correlation results from the combination of locations and does not hold within most structures (see Table S1). **E, F:** In contrast, E/N ratios are strongly correlated with endothelial cell densities locally within each structure, but different brain

structures have non-overlapping E/N ratios with similar endothelial cell densities, indicating that the apparent overall correlation does not result from a universal correlation, unlike that seen for the strong and universal correlation between E/N and neuronal density (**A, B**). All graphs are shown with similar X and Y scales for comparison.

Because of the much larger variation in neuronal densities than in endothelial cell densities across sites, the local ratio of endothelial cells per neuron is inversely proportional to local neuronal density across all sites and structures examined (Fig. 5). Importantly, this relationship is universal across brain locations, as the power function that applies across structures contains all structures and almost all data points within its 95% CI (Fig. 5A, B). That is, each neuron is accompanied by more endothelial cells at sites with lower neuronal densities than at sites with higher neuronal densities. In contrast, the ratio of endothelial cells per neuron does not vary consistently with local glial cell density neither across nor within brain structures (Fig. 5C, D). As expected for the quantity in the numerator of the ratio, local endothelial cell density is very strongly correlated with the E/N ratio in each brain structure in the mouse brain, but there is hardly any overlap across structures: because of the widely different neuronal densities across structures, brain sites with similar densities of endothelial cells have very different E/N ratios across structures (Fig. 5E, F). As could be expected of two quantities that are heavily dependent on variation in neuronal density, the E/N ratio is strongly and linearly correlated with the G/N ratio across all sites and structures (Fig. 6). That is, where more endothelial cells supply energy per neuron (i.e. in structure and sites with low neuron density), there are also more glial cells per neuron. Importantly, the relationship that applies across structures includes most data points for every structure, indicating that this relationship is universal.

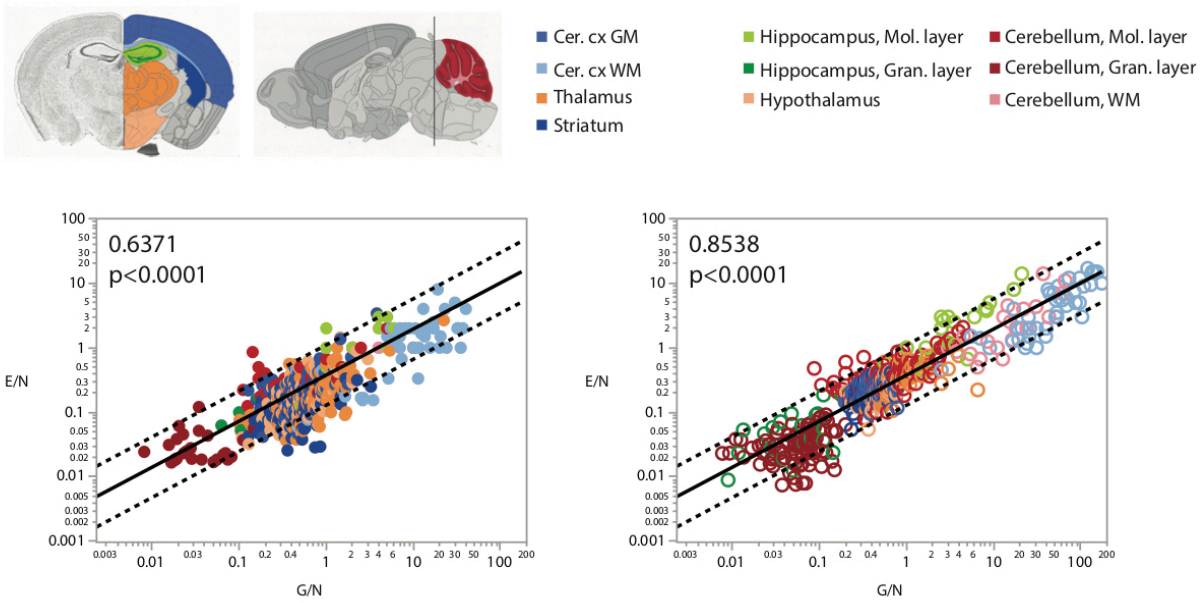

Fig. 6. More endothelial cells per neuron (E/N) are uniformly found in brain structures and sites with more glial cells per neuron, as expected given that both these variables are strongly and inversely correlated with local neuronal density (Figs. 4, 5). Spearman correlation coefficients are indicated in the graphs.

Finally, comparing our measurements of local cell densities and capillary fraction in cortical grey matter sites matching those with recently published data on local synaptic densities in the mouse cerebral cortex (*21*) we could examine whether there is evidence of higher energy availability in sites of higher synaptic densities to support the expectation that energy use increases together with synaptic activity (*3,4*; Table S6). Densities of synapses (measured as synapses that express PSD and/or SAP according to data in [*21*]) vary 1.5-fold across cortical sites, while densities of endothelial cells vary 2.5-fold and neuronal densities vary a similar 2.2-fold. However, we find no significant correlation between local endothelial cell density and synaptic density (Fig. 7A) or neuronal density (Fig. 7B) within the mouse cerebral cortex (Spearman, p=0.4133 and 0.7047), indicating that cortical sites with more synapses or more neurons receive as much capillary supply as sites with fewer synapses or neurons. Higher local synaptic densities are modestly associated with higher local neuronal densities (Fig. 7C; Spearman, p=0.0414), such that the ratio of synapses per neuron is concentrated in the 6,500-9,500 range (Fig. 7E; Spearman, p= 0.0129 due to a single data point above 12,500), compatible with previous estimates of ca. 8,000 synapses per cortical neuron in the mouse (*29,30*). We find

that the average number of synapses per neuron is not higher where there are more synapses (Fig. 7D; Spearman, p=0.0775). Crucially, the average number of synapses per neuron is not significantly correlated with the local ratio of endothelial cells per neuron (Fig. 7F; Spearman, p=0.4717): the E/N ratio varies about 4-fold across cortical sites with similar average numbers of synapses per neuron, and at a similar capillary supply per neuron, local neurons may have more or fewer synapses on average. Instead, the most striking pattern is, again, that at cortical sites where each neuron has more capillary cells available to it, there are also more capillary cells available per synapse (Fig. 7G; Spearman, p=0.0001).

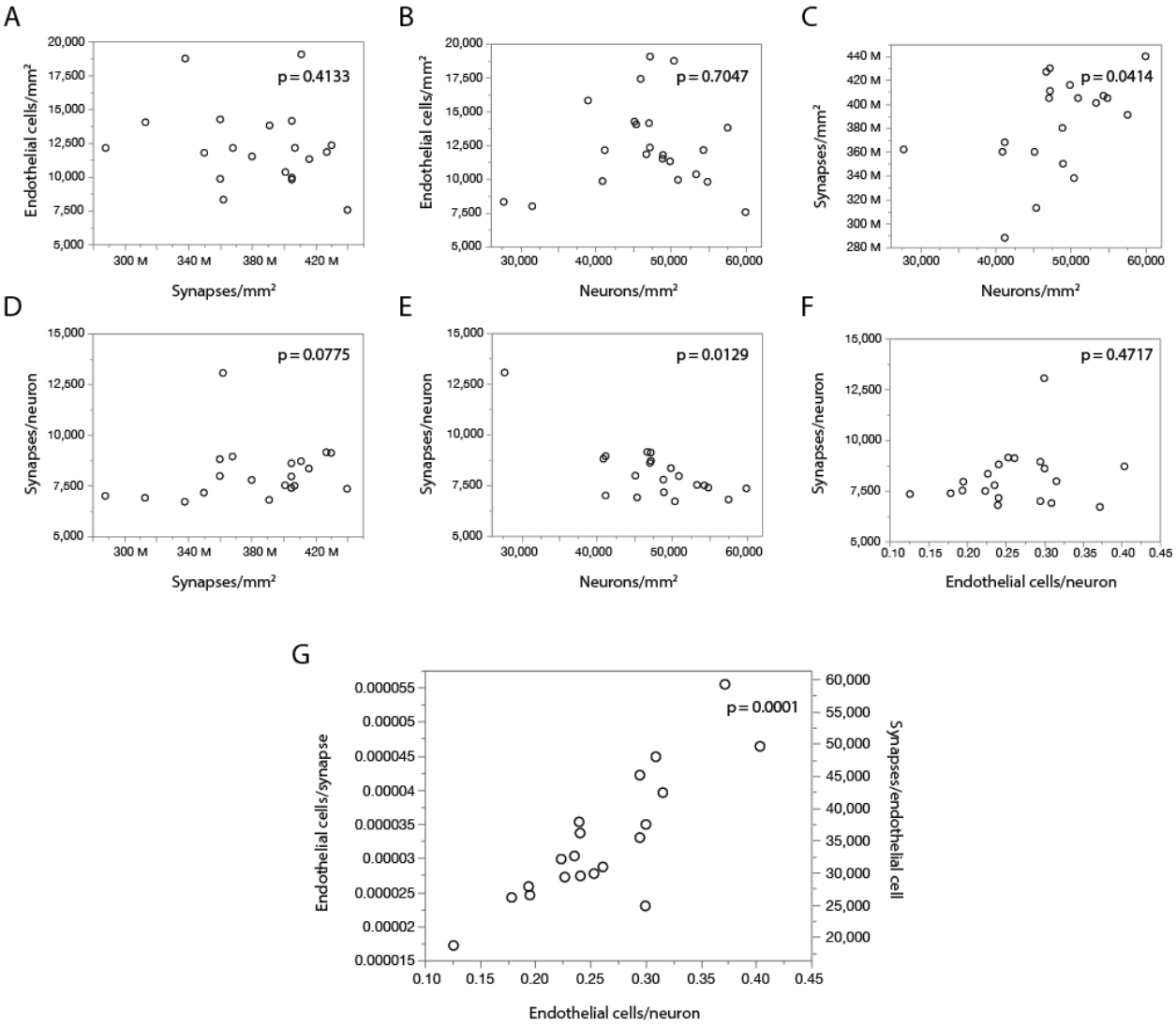

Fig. 7. With fairly constant numbers of synapses per neuron, the number of synapses served per endothelial cell increases together with the ratio of endothelial cells per neuron across sites in the mouse cerebral cortex. Data on local synaptic densities from (*21*) were combined to estimates of local densities of endothelial cells, neurons and glial cells in 2D images acquired in matching locations of the cerebral cortex as described in (*21*). Local densities of endothelial cells are not significantly correlated with local synaptic densities (**A**) or neuronal densities

(**B**). Sites with more neurons have marginally, but significantly, more synapses (**C**), which is consistent with a lack of correlation between local synaptic density and the number of synapses per neuron (**D**), although a correlation between average number of synapses per neuron and local neuronal density, due to one outlier, cannot be discarded (**E**). Still, there is very clearly no correlation between local numbers of synapses per neuron and the ratio of endothelial cells per neuron (**F**); rather, the latter is directly, and strongly (r^2=0.750), correlated with the ratio of endothelial cells per synapse (or its inverse, the number of synapses per endothelial cell; **G**). All correlation coefficients are available in Table S6.

These data thus indicate that higher E/S is associated with higher E/N, even though there are not more endothelial cells where there are more synapses (or more neurons; Fig. 7A, B), and there are also not more E/N where there are more S/N (Fig. 7F). Rather, higher E/S occurs with higher E/N (Fig. 7G) simply due to small variations in endothelial cell densities that are not correlated with variations in densities of neurons or synapses (Fig. 7A-B) in the presence of significant local variations in neuronal densities that are only somewhat correlated with smaller variations in densities of synapses (Fig. 7C). Principal component analysis supports this conclusion: three factors are required to account for the variance in all six variables, with capillary density loading only in the first factor (explaining 42.9% of variance; factor loading, 0.996, associated with E/N [0.816] and E/S [0.926]), neuronal density loading only in the second factor (total variance explained, 78.8%; loading, -0.943, associated with E/N [0.557] and S/N [0.976]), and synaptic density as the sole contributor to the third factor (explaining a total of 99.3% of variance; factor loading, 0.981).

Finally, while the glia/neuron ratio is locally higher in cortical sites where the endothelial cell/neuron ratio is also higher (Spearman, p=0.0118), the number of endothelial cells per synapse is not correlated with the local glia/neuron ratio (p=0.2868; Table S1). Thus, a higher proportion of glial cells per neuron is not associated with a larger capillary supply per synapse.

DISCUSSION

Our finding that the capillary area fraction or density of capillary cells does not accompany the enormous variation in neuronal densities across sites in the mouse brain provides evidence against several intuitive, but so far untested, central tenets of neurophysiology and functional brain imaging: that neurons *demand* energy, and larger neurons demand more than smaller neurons; that more synapses use more energy; that larger neurons have more synapses (and therefore demand more energy); and that the steady-state density of the capillary bed adjusts

itself across brain sites according to variations in energy demand. Instead, we interpret our data to indicate that due to the 100x larger variation in neuronal densities than in capillary density throughout the mouse brain, larger neurons *get access* to more energy simply because where neurons are larger, as indicated by lower neuronal densities, fewer neurons compete for the capillary density-restricted blood supply. Similarly, we propose that, given a small but significant variation in densities of synapses with densities of neurons within the cerebral cortex, there is a restricted range of numbers of synapses per neuron, and more endothelial cells providing energy both per neuron and per synapse where neurons are larger (highlighted middle panel in Fig. 1). These findings suggest the intriguing possibility that increasing neuronal sizes in evolution may have brought the advantage of increasing energy availability per individual neuron, a possibility that we are now ready to address by extending the present analysis to other species.

While we examine fixed tissue and can make no claims about physiological properties and dynamic changes in neurovascular coupling, the fairly stable distribution of the capillary bed in the perfused tissue compared to neuronal densities does inform that there is more energy available per neuron in those sites with lower neuronal densities (with few and larger neurons [*31*]) than in sites of high neuronal density. These findings are compatible with a scenario where neurons compete for a limited energy supply, rather than the usually presumed scenario in which larger neurons and/or neurons with more synapses *demand* more energy which is then provided as the capillary bed adapts to those demands during development. A limited energy supply constrained by the density of the capillary bed would have direct consequences for the level of neuronal and synaptic activity that can be sustained across brain sites, in line with our previous suggestion that fundamental aspects of neuronal structure and function are constrained by energy supply across species (*32*). It remains to be determined whether these constraints manifest themselves during development, for instance through the self-regulation of the numbers of synapses that can form and remain active, or simply through self-regulation of levels of activity (as in synaptic homeostasis; *33*).

Previous studies about microvasculature and metabolism consumption showed a linear correlation between small variations in local vascular density, blood flow, and rates of glucose utilization at rest across sites of rat brain (*8, 34, 35*). Those findings imply that capillary density and the associated, and easily measured, the density of endothelial cells in fixed brain tissue are

useful proxies of rates of blood flow and glucose utilization at rest, and therefore E/N ratios, as measured here, are useful proxies for energy availability per neuron across brain sites. Indeed, we find that the small variations in the local vascular fraction measured as in the present study across sites in the rat brain are a very good approximation of measurements of local energy cost at rest in each structure (Ventura-Antunes, Dasgupta and Herculano-Houzel, in preparation). These findings open the way to comparative studies of energy availability per neuron in brains of species that are unlikely to ever be brought alive to laboratory settings.

The present findings have fundamental implications for brain health and normal and diseased aging. First, they indicate that the heightened vulnerability of the white matter to ischemia (*36*) may be primarily due to its low capillary density compared to gray matter structures, and not simply to its large relative volume. Second, as cortical locations with high neuron densities have far less blood supplied per neuron than locations with low neuronal densities, individual neurons in "crowded" cortical areas are likely to be much more vulnerable to aging and pathologies that compromise circulation and/or metabolic capacity. Most remarkably, the hippocampus, whose granular layer contains most of its neurons and exhibits some of the lowest values of E/N found here, is one of the brain structures most highly vulnerable to hypoxia (*37*). Finally, some of the regions first and most vulnerable to Alzheimer's disease are cortical areas with high resting metabolism (38). While that might be indicative of higher capillary densities that would increase energy availability as a whole, it is possible that this is offset by very high neuronal densities, such as those found in the entorhinal cortex and hippocampus here, leading to low values of E/N. We are currently investigating the possibility that E/N correlates with brain tissue vulnerability in normal and diseased aging.

Materials and Methods

Ethics Statement: All animal used in this project was approved by the Committee on Ethical Animal Use of the Health Sciences Center (CEUA-CCS), Federal University of Rio de Janeiro (UFRJ) with protocol number: 01200.001568/2013-87.

Experimental approach: We used structured illumination confocal imaging to allow quantification of cells and microvasculature in individual sections (2D) and stacks (3D) of multiple locations in the brain of five adult mice. In two of those mice, subjected to detailed 3D quantification, brain microvasculature was revealed by injection of a fluorescent tracer (FITC-Dextran, see below) into the caudal vein; in the other three, subjected to much more time-efficient 2D quantification, brain capillaries were revealed by immunohistochemistry against collagen IV, which labels the basal lamina of blood vessels, once we established that measurements of capillary density were indistinguishable between the two labeling methods (see

below). Immunohistochemistry against the neuronal marker NeuN (*39*) was used to reveal neurons; glial cells were identified by exclusion of neurons and capillary-associated cells from the total number of cell nuclei visualized with DAPI.

Experimental animals: Five male Swiss mice aged 2.5 months were analyzed. Two mice received an injection of 200 mg/kg of fluorescein-isothiocyanate-dextran (FITC-dextran 70 kDa) in the caudal vein, to label the lumen of all blood vessels (Fig. S1). One hour after the injection, the half-life required for distribution in the lumen of blood vessels (*36*), the animals were deeply anesthetized with Xylazine (15 mg/Kg) and Ketamine (100 mg/Kg), decapitated, and their brain was quickly removed and fixed by immersion in 4% of paraformaldehyde in phosphate buffer for one hour followed by 30% sucrose in 0.1 M phosphate buffer for cryoprotection. Using a Leica microtome, the cerebellum was cut into a series of 40 µm thick sagittal sections, and the remaining tissue was cut into a series of 40 µm coronal sections. All sections were stored at -20°C in antifreeze solution (30% polyethylene glycol and 30% glycerol in 0.1 M phosphate buffer) until further use. Three other mice were similarly deeply anesthetized with Xylazine and Ketamine and perfused through the heart with 0.9% saline followed by 4% paraformaldehyde in phosphate buffer. The brain was removed and post-fixed for one hour by immersion in 4% of paraformaldehyde in phosphate buffer, then sectioned as above.

Immunofluorescence: One in every six sections of each brain was subjected to immunohistochemistry and counterstaining with DAPI. Anti-NeuN antibody was used to reveal neurons; additionally, those sections from the three animals not injected with FITC-Dextran were subjected to immunohistochemistry against collagen IV to reveal cell nuclei intimately associated with capillaries.

Each section was washed in phosphate buffer (PB) for five minutes, heat for one hour at 70 °C in a 0.1 M solution of boric acid, pH 9.0, then incubated for one hour in PB containing 3% normal goat serum (Sigma-Aldrich, LG9023) and 2% bovine serum albumin (Sigma-Aldrich- A2058). Sections from animals not injected with FITC-Dextran were next incubated under stirring for 48 hours at 4°C in PB containing rabbit polyclonal anti-collagen IV antibody (Abcam, Ab6586) at a 1:500 dilution. Each section was then washed three times in PB for 5 minutes each and incubated for 2 hours at 4°C in a 1:500 dilution of Alexa Fluor 488 goat anti-rabbit secondary antibody (Abcam, Ab150077). From this step on, all brain sections were treated similarly: washed three times in PB and incubated for 24 hours at 4°C under continuous stirring with rabbit primary polyclonal antibody against Cy3-conjugated NeuN (Millipore, ABN78C3) diluted 1:1000 in PB. All sections were then labeled with DAPI (4',6-Diamidino-2-Phenylindole Dilactate, from stock solution at 20 mg/l) to provide counter-staining for identification of brain structures and allow visualization of all cell nuclei in each section. The sections were then mounted on glass slides and coated with Vectashield (Vector Labs, Cat. number H-1400) for viewing under fluorescence microscopy.

Structures analyzed: Ten structures of interest were targeted for analysis: gray matter (GM) and white matter (WM) of the cerebral cortex; striatum; thalamus; hypothalamus; granular and molecular layers of the hippocampal dentate gyrus; white matter and granular and molecular layers of the cerebellum. Structures were defined according to the Mouse Brain Atlas (*40*).

Microscopy: A Zeiss AxioImager M2 microscope equipped with an Apotome 2 for confocal imaging under structured illumination (Carl Zeiss, Jena, Germany) and driven by

StereoInvestigator software (Microbrightfield Bioscience, Williston, VT) was used for all image acquisition.

We first delineated the boundaries of the ten brain structures of interest in each section. For each structure, image stacks for 3D analysis were acquired using systematic random sampling in StereoInvestigator under magnification with a 63x (Plan-ApoChromat), which gives a depth of field of 0.5 µm with oil, with an optical plane of 0.5 µm and step size of 0.5 µm. Stacks were 1388 x1040 µm wide x 30 µm thick and typically contained 60 images each, spanning most of the full mounted thickness of the section. Within each stack, 3D counting probes placed were variable in size according to the structure (Table S1) and were placed to exclude the sectioned surfaces and zones outside the structure of interest (Fig. S1). The grey matter of the cerebellar cortex was imaged as a whole and analyzed separately into molecular and granular layers. For 2D analysis, image composites of the entire brain sections were acquired under 20x magnification (EC Plan-NeoFluar/420350-9900), which gives a thicker depth of field of ca. 4 µm, and counting probes consisted of rectangular regions of interest (ROIs) placed to cover large areas of the target structures in each brain section (see Fig. S2). In the cerebral cortex, rectangular probes spanned the entire grey matter from pia to the white matter border, and 5-15 probes of ca. 800 µm width were placed at regular intervals along each section. For all other structures, 2-8 rectangular probes were placed in each section, seeking to maximize the sampled surface of each structure (Fig. S2A).

Although highly time-consuming, detailed analysis of 3D images was performed first to rule out bias in data acquisition due to any preferential organization of capillaries relative to the plane of section, given the three-dimensional nature of the distribution of the capillary network. To ensure feasibility of future analyses of a large number of species, and to allow for a much larger sample size, we compared the results of the 3D analysis of small image stacks with the much faster and more practical analysis of 2D image composites, which permitted the analysis of much larger ROIs and numbers of cells in half as much time. Those analyses had to be performed in separate animals due to bleaching of the immunofluorescence during acquisition of image stacks. Due to software limitations that precluded acquiring large composites at 63x, 2D image composites had to be acquired at 20x, which leads to inflated estimates of area (or volume) fraction occupied by capillaries due to the projection of oblique vessels given the larger thickness of the optical sections at 20x (ca. 4 mm) compared to 63x (ca. 0.5 mm). For the same reason, estimates of local cell densities will also differ between the two methods. However, we hypothesize that all relationships across variables should remain unaffected by the method of image acquisition. All results are thus presented side by side for 3D and 2D analyses. Data points overlap across animals (shown in different symbols in all figures), and are thus analyzed jointly.

3D analysis: Stacks in the targeted brain structures of two FITC-injected mice were acquired using systematic random sampling (SRS) of each structure in each of 1 of 6 sections. From each brain, 13 and 18 sagittal sections through the cerebellum and 24 and 23 coronal sections through the remaining brain structures, including the cerebrum, were analyzed. A total of 867 stacks were analyzed across the ten brain structures in two mice (Table S2, mouse 01 and mouse 02).

2D analysis: From each of three animals, 21, 12 and 17 sections through the cerebellum and 21, 20 and 14 sections through the remaining brain structures were analyzed. A total of 750 ROIs were imaged and analyzed across the ten brain structures (Table S2, mice 03-05).

Image analysis: In each stack and ROI analyzed, we manually identified each DAPI-stained cell nucleus in the structure site as neuronal (when it expressed NeuN immunoreactivity), endothelial or belonging to other capillary-associated cells (when the cell was intimately associated with FITC-labeled capillary lumen or collagen IV-stained basal lamina, which includes pericytes), or glial (by exclusion; Fig. S2B).

Microvascular area fraction (hereafter termed "capillary area fraction" for simplicity) was estimated in image stacks and 2D ROIs using the Cavalieri estimator in StereoInvestigator using a grid of points separated by 2 µm in 3D images and 4 µm in 2D images (Figure 2C). Capillary *area* and *volume* fraction are interchangeable (*41*) and refer to the fraction of tissue formed by endothelial cells and the lumen of the capillaries that they form. In order to restrict analysis to capillaries, where stacks included large vessels, the counting probe was reduced to avoid it, or else the stack was discarded. In 2D, ROIs were placed to avoid large vessels.

Labeling capillaries with FITC-dextran or immunohistochemistry to collagen IV is expected to lead to slightly different measurements of capillary density expressed as area (or volume) fraction, because while the former labels the lumen of blood vessels, the latter labels the basal lamina of the cells that form the walls of the vessels. However, estimates of numbers of capillary-associated cells per site should remain unaffected. To evaluate how much the difference in measured capillary volume fraction depending on staining method would impact our results, one additional 1-in-6 series of brain sections of mouse #01, which received the injection of FITC-Dextran, were double-labeled for collagen IV using the same primary antibody as before, but a different secondary antibody, conjugated to Alexa Fluor 546 (1:500/#A11010 - Life). Fig. S2D illustrates the coincident but non-overlapping double labeling of lumen and basal lamina of the microvasculature and the associated DAPI-stained cell nuclei. Quantification of the area fraction covered by capillaries in 2D composites acquired at 20x showed a detectable but not statistically significant difference between the vascular fraction estimated with collagen IV (7.4±0.3%) compared to FITC-Dextran (6.6±0.4%).

Correlations with synaptic density: In order to determine whether local densities of synapses correlate with local densities of neurons and capillaries and to establish how variable are the ratios of synapses per neuron and number of synapses supplied per capillary cell, we proceeded with the quantification of four sections from the brain of mouse #4 that matched the respective levels of the four coronal sections through the cerebral cortex of one individual mouse in the synaptome study of Zhu et al. (*21*). We used the Mouse Brain Atlas (Franklin and Paxinos) to place large ROIs in the same structures. 2D composite images acquired under 20x magnification were analyzed to determine the density of cells and vascular fraction of neocortex in our images for comparison with the total number of synapses labeled with either PSD95 or SAP (*21*).

Statistical analysis: All analyses were performed in JMP14 PRO, using non-parametric Spearman correlation coefficients to test the correlation between variables, and regression to mathematical functions to determine the type of relationship between variables.

Acknowledgments: Thanks to Louise Botelho, Felipe Tenório and Marina Ricardo for contributing to image analysis, and to Prof. Doug Rothman for insightful discussions. This work was supported by a Scholar Award from the James S. McDonnell Foundation and Vanderbilt start-up funds to SHH, and by a CAPES fellowship to LVA. SHH conceived the study, LVA executed all data acquisition, and both authors analyzed data and wrote the manuscript. Authors

declare no competing interests. Raw data tables are available in XLS and JMP formats upon request.

References and notes

1. Rolfe DFS, Brown GC (1997) Cellular energy utilization and molecular origin of standard metabolic rate in mammals. Physiol Rev 77, 731-758
2. Aschoff J, Günther B, Kramer K (1971) Energiehaushalt und Temperaturregulation. Urban and Schwarzenberg, Munich.
3. Attwell D, Laughlin SB (2001) An energy budget for signaling in the grey matter of the brain. J Cereb Blood Flow Metab 21: 1133–1145.
4. Harris JJ, Jolivet R, Attwell D (2012) Synaptic energy use and supply. Neuron 75, 762-777.
5. Ames III A (2000) CNS energy metabolism as related to function. Brain Res Rev 34, 42-68.
6. Magistretti PJ (2006) Neuron-glia metabolic coupling and plasticity. J Exp Biol 209, 2304-2311.
7. Pellerin L, Magistretti PJ (2016) Neuroenergetics: calling upon astrocytes to satisfy hungry neurons. The Neuroscientist 10, 53-62.
8. Klein B, Kuschinsky W, Schrock H, Vetterlein F (1986). Interdependency of local capillary density, blood flow, and metabolism in rat brains. American Journal of Physiology-Heart and Circulatory Physiology 25, H1333-H1340.
9. Noda A, Ohba H, Kakiuchi T, et al. (2002) Age-related changes in cerebral blood flow and glucose metabolism in conscious rhesus monkeys. Brain Research 936:76–81.
10. Leach RM, Treacher DF (1998) Oxygen transport – 2. Tissue hypoxia. BMJ 317, 1370-1373.
11. Alle H, Roth A, Geiger JR. (2009) Energy-efficient action potentials in hippocampal mossy fibers. Science 325, 1405-1408.
12. Howarth C, Peppiatt-Wildman CM, Attwell D (2010) The energy use associated with neural computation in the cerebellum. J Cereb Blood Flow Metab 30, 403-414.
13. Hainsworth FR, Collins BG, Wolf LL (1977) The function of torpor in hummingbirds. Physiol Biochem Zool 50, 215-222.
14. Banavar JR, Damuth J, Maritan A, Rinaldo A (2002) Supply-demand balance and metabolic scaling. Proc Natl Acad Sci 99, 10506-10509.
15. Leithner C, Royl G (2014) Oxygen paradox of neurovascular coupling. Journal of Cerebral Blood Flow and Metabolism 34, 19-29.
16. Schölvinck ML, Howarth C, Attwell D (2008) The cortical energy needed for conscious perception. Neuroimage 40, 1460-1468.

17. Lin AL, Fox PT, Hardies J, Duong TQ, Gao JH (2010) Nonlinear coupling between cerebral blood flow, oxygen consumption, and ATP production in human visual cortex. Proc Natl Acad Sci USA 107, 8446-8451.
18. Hudetz AG (1997) Blood flow in the cerebral capillary network: a review emphasizing observations with intravital microscopy. Microcirculation 4, 233-252.
19. Mink JW, Blumenschine RJ, Adams DB (1981) Ratio of central nervous system to body metabolism in vertebrates: its constancy and functional basis. Am J Physiol Reg Integr Comp Physiol 241, R203-R212.
20. Karbowski J (2007) Global and regional brain metabolic scaling and its functional consequences. BMC Biol 5, 18.
21. Zhu F, Cizeron M, Qiu Z, Benavides-Piccione R, Kopanitsa MV, Skene NG, Koniaris B, Defelipe J, Fransé E, Komiyama NH, Grant SGN (2018) Architecture of the mouse brain synaptome. Neuron 99, 781-799.
22. Tsai PS, Kaufhold JP, Blinder P, Friedman B, Drew PJ, Karten HJ, ...Kleinfeld D (2009) Correlations of neuronal and microvascular densities in murine cortex revealed by direct counting and colocalization of nuclei and vessels. J Neurosci 29, 14553-14570.
23. Boero JA, Ascher J, Arregui A, Rovainen C, Woolsey TA (1999) Increased brain capillaries in chronic hypoxia. J Appl Physiol 86, 1211-1219.
24. Pawlik G, Rackl A, Bing RJ (1981) Quantitative capillary topography and blood flow in the cerebral cortex of cats: an in vivo microscopic study. Brain Res 208, 35-58.
25. Lauwers F, Cassot F, Lauwers-Cances V, Puwanarajah P, Duvernoy H (2008) Morphometry of the human cerebral cortex microcirculation: general characteristics and space-related profiles. Neuroimage 39, 936-948.
26. Herculano-Houzel S, Manger PR, Kaas JH (2014) Brain scaling in mammalian evolution as a consequence of concerted and mosaic changes in numbers of neurons and average neuronal cell size. Front Neuroanat 8, 77.
27. Ribeiro PFM, Ventura-Antunes L, Gabi M, Mota B, Grinberg LT, Farfel JM, Ferretti-Rebustini REL, Leite REP, Filho WJ, Herculano-Houzel S (2013) The human cerebral cortex is neither one nor many: neuronal distribution reveals two quantitatively different zones in the gray matter, three in the white matter, and explains local variations in cortical folding. Front Neuroanat 7, 28.
28. Herculano-Houzel S, Watson C, Paxinos G (2013) Distribution of neurons in functional areas of the mouse cerebral cortex reveals quantitatively different cortical zones. Front Neuroanat 7, 35.

29. Schüz, A., & Palm, G. (1989). Density of neurons and synapses in the cerebral cortex of the mouse. Journal of Comparative Neurology, 286(4), 442-455.
30. Braitenberg V, Schüz A (1998) Cortex: Statistics and geometry of neuronal connectivity. Berlin: Springer.
31. Mota B, Herculano-Houzel S (2014) All brains are made of this: a fundamental building block of brain matter with matching neuronal and glial masses. Front Neuroanat 8, 127.
32. Herculano-Houzel S (2011) Scaling of brain metabolism with a fixed energy budget per neuron: implications for neuronal activity, plasticity and evolution. PloS One 6, e17514.
33. Turrigiano G (2012) Homeostatic synaptic plasticity: local and global mechanisms for stabilizing neuronal function. Cold Spring Harbor Perspectives in Biology 4, a005736.
34. Borowsky IW, Collins RC (1989) Metabolic anatomy of brain: a comparison of regional capillary density, glucose metabolism, and enzyme activities. Journal of Comparative Neurology 288, 401-413.
35. Kuschinsky W, Paulson OB (1992) Capillary circulation in the brain. Cerebrovascular and Brain Metabolism Reviews 4, 261-286.
36. Wang Y, Liu G, Hong D, Chen F, Ji X, Cao G (2016) White matter injury in ischemic stroke. Prog Neurobiol 141, 45-60.
37. Hossmann KA (1999) The hypoxic brain. Insights from ischemia research. Adv Exp Med Biol 474, 155-169.
38. Buckner RL, Snyder AZ, Shannon BJ, LaRossa G, Sachs R, Fotenos AF, Sheline YI, Klunk WE, Mathis CA, Morris JC, Mintun MA (2005) Molecular, structural, and functional characterization of Alzheimer's disease: Evidence for a relationship between default activity, amyloid, and memory. Journal of Neuroscience 25, 7709-7717.
39. Mullen RJ, Buck CR, Smith AM (1992) NeuN, a neuronal specific nuclear protein in vertebrates. Development 116, 201-211.
40. Franklin K, Paxinos G (1997) The mouse brain in stereotaxic coordinates. New York, Elsevier.
41. Gundersen HJ, Jensen EB, Kieu K, Nielsen J (1999)The efficiency of systematic sampling in stereology – reconsidered. J Microsc 193, 199-211.

Table S1: Size of 3D counting probes per structure. CerCx, cerebral cortex; GM, gray matter; WM, white matter; GL, granular cell layer; ML, molecular cell layer.

CerCx GM	X 127 y 96 z 20 µm
CerCx WM	x 80 y 75 z 20 µm
Thalamus	x 100 y 95 z 20 µm
Hypothalamus	x 100 y 95 z 20 µm
Striatum	x 100 y 95 z 20 µm
Hippocampus ML	x 40 y 40 z 20 µm
Hippocampus GL	x 30 y 30 z 20 µm
Cerebellum GK	x 40 y 40 z 20 µm
Cerebellum ML	x 40 y 40 z 20 µm
Cerebellum WM	x 40 y 40 z 20 µm

Table S2: Numbers of cells, stacks and ROIs analyzed in each of ten structures of interest in the mouse brain.

CerCx, cerebral cortex; GM, gray matter; WM, white matter; GL, granular cell layer; ML, molecular cell layer.

Structure	Mouse 01	Mouse 02	Mouse 03	Mouse 04	Mouse 05
CerCx, GM	32 stacks 2,516 cells	54 stacks 3,495 cells	76 ROI 63,022 cells	57 ROI 17,613 cells	34 ROI 12,053 cells
CerCx, WM	60 stacks 1,497 cells	69 stacks 2,531 cells	59 ROI 2,651 cells	19 ROI 1,636 cells	27 ROI 3,931 cells
Thalamus	83 stacks 4,349 cells	42 stacks 1,997 cells	21 ROI 9,096 cells	15 ROI 5,442 cells	16 ROI 3,634 cells
Hypothalamus	45 stacks 2,816 cells	34 stacks 1,861 cells	13 ROI 5,358 cells	12 ROI 2,260 cells	11 ROI 2,125 cells
Striatum	59 stacks 3,283 cells	43 stacks 2,693 cells	29 ROI 15,539 cells	16 ROI 6,284 cells	18 ROI 6,467 cells
Hippocampus, ML	40 stacks 137 cells	73 stacks 202 cells	9 ROI 136 cells	9 ROI 88 cells	8 ROI 118 cells
Hippocampus, GL	25 stacks 470 cells	21 stacks 368 cells	13 ROI 726 cells	13 ROI 310 cells	9 ROI 609 cells
Cerebellum, GL	37 stacks 2,105 cells	23 stacks 1,167 cells	43 ROI 16,850 cells	22 ROI 4,084 cells	34 ROI 5,892 cells
Cerebellum, ML	41 stacks 361 cells	26 stacks 179 cells	42 ROI 3,982 cells	23 ROI 1,313 cells	35 ROI 1,632 cells
Cerebellum, WM	32 stacks 138 cells	28 stacks 105 cells	29 ROI 1,746 cells	15 ROI 778 cells	23 ROI 831 cells
Total	454 stacks 17,672 cells	413 stacks 14,598 cells	334 ROI 119,106 cells	201 ROI 39,808 cells	215 ROI 37,292 cells

Table S3. Fractional cellular composition of different structures of the mouse brain. V, quantified in 3Dalues correspond to the average across sites in each structure of two mice (#1 and #2). CerCx, cerebral cortex; GM, gray matter; WM, white matter; GL, granular cell layer; ML, molecular cell layer; Cb, cerebellum.

3D	% capillary fraction	% endothelial cells	% neurons	% glial cells	Glial cells % of non-neuronal cells
CerCx, GM	2.22 ± 0.11%	13.90 ± 0.79%	57.86 ± 1.53%	28.22 ± 1.23%	66.64 ± 1.49%
CerCx, WM	0.75 ± 0.03%	7.62 ± 0.60%	5.75 ± 1.15%	82.61 ± 1.41%	91.37 ± 0.76%
Striatum	1.43 ± 0.06%	7.94 ± 0.34%	62.47 ± 1.10%	29.57 ± 1.10%	77.58 ± 0.99%
Thalamus	1.35 ± 0.05%	10.74 ± 0.52%	51.24 ± 1.31%	38.01 ± 1.2%	77.31 ± 1.00%
Hypothalamus	1.34 ± 0.06%	10.14 ± 0.69%	60.62 ± 1.61%	29.23 ± 1.36%	73.34 ± 1.64%
DG, GL	0.70 ± 0.07%	1.46 ± 0.47%	94.96 ± 1.08%	3.57 ± 0.92%	67.46 ± 9.30%
DG, ML	1.10 ± 0.06%	29.18 ± 3.21%	10.33 ± 3.29%	60.48 ± 3.29%	68.23 ± 3.35%
Cb, GL	1.56 ± 0.06%	2.58 ± 0.33%	95.44 ±0.46%	1.96 ±0.33%	38.86 ± 5.06%
Cb, ML	1.69 ± 0.09%	13.92 ± 3.76%	59.77 ± 3.90%	26.30 ± 3.76%	54.35 ± 4.93%
Cb, WM	1.25 ± 0.06%	14.14 ± 2.68%	0.73 ± 0.52%	85.12 ± 2.76%	85.64 ± 2.69%

Table S4. Fractional cellular composition of different structures of the mouse brain, quantified in 2D. Values correspond to the average across sites in each brain structure of three mice (#3, #4 and #5). *Note that the capillary fraction appears higher here than when measured in 3D due to the deeper focal thickness under the lower magnification used for 2D image acquisition, which artificially inflates the relative capillary fraction. Other values are similar between 2D and 3D estimates.

2D	% capillary fraction*	% endothelial cells	% neurons	% glial cells	Glial cells % of non-neuronal cells
CerCx, GM	8.65 ± 0.21%	14.37 ± 0.23%	60.86 ± 0.39%	24.75 ± 0.36%	63.06 ± 0.53%
CerCx, WM	5.35 ± 0.27%	10.63 ± 0.55%	2.99 ± 0.93%	86.37 ± 1.18%	88.55 ± 0.75%
Striatum	7.74 ± 0.25%	11.88 ± 0.37%	63.59 ± 0.83%	24.51 ± 0.71%	67.14 ± 0.88%
Thalamus	7.58 ± 0.71%	14.53 ± 0.71%	45.88 ± 1.89%	39.57 ± 1.90%	72.19 ± 1.30%
Hypothalamus	7.28 ± 0.39%	12.38 ± 0.63%	57.13 ± 1.60%	30.47 ± 1.34%	70.77 ± 1.40%
DG, GL	6.17 ± 0.06%	4.55 ± 0.72%	90.89 ± 1.46%	4.55 ± 0.89%	46.32 ± 5.72%
DG, ML	10.91 ± 0.91%	30.67 ± 1.70%	13.17 ± 2.34%	56.15 ± 2.34%	64.43 ± 1.93%
Cb, GL	6.76 ± 0.26%	3.02 ± 0.17%	91.00 ± 0.47%	5.97 ± 0.38%	63.22 ± 1.83%
Cb, ML	7.20 ± 0.25%	18.77 ± 0.62%	47.02 ± 1.57%	34.20 ± 1.48%	62.47 ± 1.48%
Cb, WM	4.16 ± 0.22%	13.50 ± 0.77%	2.34 ± 0.56%	84.14 ± 0.95%	86.13 ± 0.79%

Table S5. Correlation coefficients and power exponents for Figures 2-6: Please see xls file attached.

Table S6. Spearman correlation coefficients and p-values for correlations across cerebral cortical sites. DE, local density of endothelial cells; DN, local neuronal density; DG, local density of glial cells; DS, local density of synapses; E/N, ratio of endothelial cells per neuron; E/G, ratio of endothelial cells per glial cell; E/S, ratio of endothelial cells per synapse; G/N, ratio of glial cells per neuron; S/N, ratio of synapses per neuron; S/G, ratio of synapses per glial cell. All values pertaining to DE, DN and DG were obtained in the present study, from analysis of 2D images acquired in locations matching those described in (*21*); all values pertaining do DS were calculated from (*21*).

	D_E	D_N	D_G	D_S	E/N	E/G	E/S	G/N	S/N	S/G
D_E		-0.084, 0.7047	0.412, 0.0509	-0.194, 0.4133	**0.753, <0.0001**	**0.741, <0.0001**	**0.906, <0.0001**	0.123, 0.5758	-0.166, 0.4837	-0.393, 0.0862
D_N	-0.084, 0.7047		0.307, 0.1542	*0.460, 0.0414*	**-0.652, 0.0007**	-0.121, 0.5820	-0.235, 0.3177	**-0.624, 0.0015**	**-0.545, 0.0129**	0.056, 0.8113
D_G	0.412, 0.0509	0.307, 0.1542		0.108, 0.6488	0.128, 0.5605	-0.203, 0.3525	0.312, 0.1803	*0.441, 0.0350*	-0.291, 0.2131	**-0.831, <0.0001**
D_S	-0.194, 0.4133	*0.460, 0.0414*	0.108, 0.6488		-0.441, 0.0517	-0.215, 0.3632	**-0.506, 0.0230**	-0.306, 0.1896	0.404, 0.0775	0.363, 0.1156
E/N	**0.753, <0.0001**	**-0.652, 0.0007**	0.128, 0.5605	-0.441, 0.0517		**0.630, 0.0013**	**0.750, 0.0001**	**0.516, 0.0118**	0.171, 0.4717	-0.306, 0.1893
E/G	**0.741, <0.0001**	-0.121, 0.5820	-0.203, 0.3525	-0.215, 0.3632	**0.630, 0.0013**		**0.628, 0.0030**	-0.273, 0.2069	0.435, 0.0555	0.252, 0.2838
E/S	**0.906, <0.0001**	-0.235, 0.3177	0.312, 0.1803	**-0.506, 0.0230**	**0.750, 0.0001**	**0.628, 0.0030**		0.250, 0.2868	-0.364, 0.1163	**-0.526, 0.0171**
G/N	0.123, 0.5758	**-0.624, 0.0015**	*0.441, 0.0350*	-0.306, 0.1896	**0.516, 0.0118**	-0.273, 0.2069	0.250, 0.2868		0.235, 0.3177	**-0.669, 0.0013**
S/N	-0.166, 0.4837	**-0.545, 0.0129**	-0.291, 0.2131	0.404, 0.0775	0.171, 0.4717	0.435, 0.0555	-0.364, 0.1163	0.235, 0.3177		0.435, 0.0555
S/G	-0.393, 0.0862	0.056, 0.8113	**-0.831, <0.0001**	0.363, 0.1156	-0.306, 0.1893	0.252, 0.2838	**-0.526, 0.0171**	**-0.669, 0.0013**	0.435, 0.0555	